Published in final edited form as:
ACS Chem Biol. 2021 November 19; 16(11): 2401–2414. doi:10.1021/acschembio.1c00535.

The Coenzyme A Level Modulator Hopantenate (HoPan) Inhibits Phosphopantotenoylcysteine Synthetase Activity

Konrad J. Mostert[1,†], **Nandini Sharma**[2,†], **Marianne van der Zwaag**[3,†], **Roxine Staats**[1], **Lizbé Koekemoer**[1], **Ruchi Anand**[2], **Ody C.M. Sibon**[3], **Erick Strauss**[1,*]

[1]Department of Biochemistry, Stellenbosch University, Stellenbosch, 7600, South Africa.

[2]Department of Chemistry, Indian Institute of Technology Bombay, Mumbai-400076, India.

[3]Department of Biomedical Sciences of Cells and Systems, University Medical Center Groningen, University of Groningen, 9713 AV, The Netherlands.

Abstract

The pantothenate analogue hopantenate (HoPan) is widely used as a modulator of coenzyme A (CoA) levels in cell biology and disease models—especially for pantothenate kinase associated neurodegeneration (PKAN), a genetic disease rooted in impaired CoA metabolism. This use of HoPan was based on reports that it inhibits pantothenate kinase (PanK), the first enzyme of CoA biosynthesis. Using a combination of *in vitro* enzyme kinetic studies, crystal structure analysis, and experiments in a typical PKAN cell biology model, we demonstrate that instead of inhibiting PanK, HoPan relies on it for metabolic activation. Once phosphorylated, HoPan inhibits the next enzyme in the CoA pathway—phosphopantothenoylcysteine synthetase (PPCS)—through formation of a non-productive substrate complex. Moreover, the obtained structure of the human PPCS in complex with the inhibitor and activating nucleotide analogue provides new insights into the catalytic mechanism of PPCS enzymes—including the elusive binding mode for cysteine—and reveals the functional implications of mutations in the human PPCS that have been linked to severe dilated cardiomyopathy. Taken together, this study demonstrates that the molecular mechanism of action of HoPan is more complex than previously thought, suggesting that the results of studies in which it is used as tool compound must be interpreted with care. Moreover, our findings provide a clear framework for evaluating the various factors that contribute to the potency of CoA-directed inhibitors, one that will prove useful in the future rational development of potential therapies of both human genetic and infectious diseases.

---

[*] **Contact information** Erick Strauss (contact corresponding author): estrauss@sun.ac.za, Phone: +27-21-808-5866, Fax: +27-21-808-5863.

[†] These authors contributed equally.

Author Contributions

K.J.M., N.S., M.v.d.Z., R.S. and L.K. performed research; K.J.M., N.S., M.v.d.Z., R.A., O.C.M.S and E.S. analyzed data; R.A., O.C.M.S and E.S. provided supervision; R.A. and E.S. obtained funding; E.S. wrote the paper with reviewing and editing input from all the authors. K.J.M., N.S. and M.v.d.Z. contributed equally to the study.

The authors declare no competing interests.

ASSOCIATED CONTENT

Supporting Information

The Supporting Information is available free of charge at https://pubs.acs.org/doi/10.1021/acschembio.1c00535.

- Supplementary Figures as referenced in the manuscript, Supplementary Table containing the crystallographic data statistics of the structure reported in this study, and Supplementary Results & Discussion detailing how the hPPCS ternary structure allows for the mapping of mutations linked to severe dilated cardiomyopathy (PDF).

Graphical Abstract

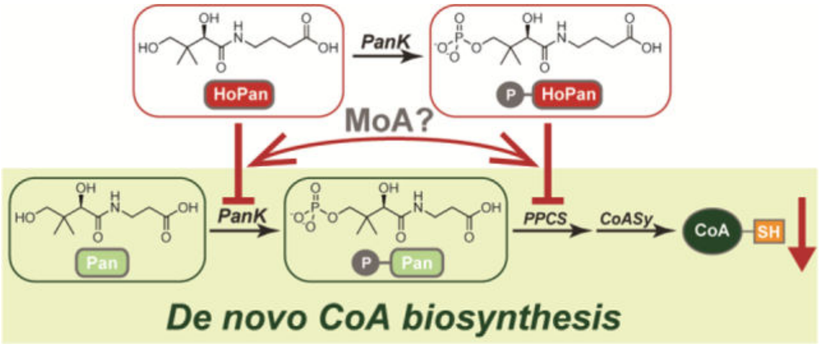

INTRODUCTION

The essential metabolic cofactor coenzyme A (CoA) plays a central role in a diversity of metabolic processes, with an estimation that up to 9% of all enzyme activities use CoA in some form.[1] In addition, it also serves as the carrier of the acetyl group that is transferred in acetylation-based signaling and regulation, such as histone acetylation.[2] It is therefore unsurprising that several genetic diseases correlate with errors in CoA biosynthesis and/or utilization,[3–5] and that manipulation of CoA, acetyl-CoA or other acyl-CoA levels offers therapeutic potential in human health through pharmaceutical intervention.[6] However, pursuing such interventions require a clear knowledge of their mode of action (MoA) to prevent the proposal of drug development strategies that would produce compounds that are not on target.

Since pantothenic acid (Pan, vitamin B$_5$, **3**) is the precursor of *de novo* CoA biosynthesis in all organisms (Figure 1), there has been much interest in the development and therapeutic use of Pan analogues, especially as antimicrobial agents.[7] Homopantothenic acid, also called hopantenic acid or hopantenate (HoPan, **1**) among several other names, is a Pan analogue in which the β-alanine moiety of the parent molecule has been exchanged for γ-aminobutyric acid (GABA) (Figure 1). Interestingly, while the molecule was first made and tested as a possible antibacterial in 1944,[8] the discovery of its ability to cross the blood-brain barrier and to act as neurological stimulant (later attributed to it acting as activator of GABA-receptors) led to its repurposing as an anticonvulsant and nootropic agent, especially in Japan and countries previously associated with the Soviet Union (in the latter case under the brand name Pantogam).[9,10] Importantly, when HoPan was administered to mice more than 90% was found to be excreted in an unmodified form,[11] with no evidence of chronic toxicity in rats.[12] Consequently, HoPan seemed to show little promise as modulator of CoA-related metabolism.

This changed with a report that HoPan acted as an inhibitor of pantothenate kinase (PanK), the first enzyme of *de novo* CoA biosynthesis that catalyzes the phosphorylation of Pan to form P-Pan (**4**) (Figure 1).[13] HoPan treatment was found to result in large decreases in CoA levels in isolated hepatocytes, and HoPan administration (100 μg/g/day) proved to be lethal within 5 days for males and 15 days for females in mice maintained on a diet without any Pan supplement. This correlated with a significant decline in a total and free CoA in especially the livers of treated animals. Importantly, the toxicity was reversed when HoPan was co-administered with Pan. This is consistent with HoPan's inhibition of CoA's biosynthesis from Pan, and also explains why previous studies—in which standard Pan-rich diets were used—showed no toxic effects for HoPan treatment.

Following this foundational study, HoPan has become the main small molecule tool compound for modulating CoA levels in a variety of model systems, including the fruit fly *Drosophila melanogaster,* mice and various cell cultures, specifically in studies of rare genetic neurodegenerative diseases linked to errors in CoA biosynthesis.[14–17] Chief among these is pantothenate kinase associated neurodegeneration (PKAN), a disease caused by certain mutations in *PANK2*, the gene encoding the human mitochondrial PanK isoform PANK2. In this context HoPan seems to be an especially appropriate tool compound based on the understanding that it reduces CoA levels by inhibiting PanK.

However, several unrelated findings, when taken together, have suggested that HoPan's MoA may be more complex. First, the study that identified HoPan as a PanK inhibitor also showed that murine hepatocytes are able to transform [^{3}H]HoPan into radiolabeled 4′-phospho-hopantenate (P-HoPan, **2**), suggesting that HoPan is also a substrate of PanK (Figure 1).[13] Second, we previously demonstrated that the addition of pantethine—the disulfide of the CoA degradation product pantetheine (PantSH, **6**)—reverses HoPan-mediated CoA depletion in *D. melanogaster*.[14] A simple explanation for this observation is that the *D. melanogaster* PanK (dPANK, also known as fumble or Fbl) is not inhibited by HoPan, and that dPanK (like other homologous type II PanKs and microbial type I PanKs) is able to phosphorylate PantSH to form 4′-phosphopantetheine (P-PantSH, **7**) in a CoA salvage pathway (Figure 1).[16,18–21] Formation of P-PantSH in this manner would bypass the phosphopantothenoylcysteine synthetase (PPCS) and phosphopantothenoylcysteine decarboxylase (PPCDC) steps of CoA biosynthesis, and would consequently show rescue if either of these activities is the molecular target of HoPan. Alternatively, if PantSH is degraded to Pan, the elevated levels of the natural PanK substrate may also provide rescue of HoPan's inhibition of dPANK. To be able to distinguish between these various hypotheses would require a kinetic analysis of dPANK's activity towards Pan and PantSH and the impact of HoPan thereon. However, no detailed comparative kinetic analysis of any eukaryotic PanK has been reported to date.

These findings prompted us to revisit the mechanism by which HoPan causes the lowering of CoA levels. In particular, HoPan's apparent phosphorylation by PanK would suggest it has a MoA similar to that of the natural product antibiotic CJ-15,801, a fungal metabolite that selectively inhibits the growth of *Staphylococcus aureus* following its phosphorylation by *S. aureus* PanK and subsequent inhibition of its PPCS (Figure 1). In this alternative mode of action HoPan would therefore not target PanK for inhibition but require it for metabolic activation; such a proposal would be consistent with all the previously published data.

We therefore set out to use biochemical, structural and genetic studies to elucidate the molecular mechanism of action (MOA) of HoPan with the goal of providing clarity regarding the results of those studies in which it is used as tool compound. In addition, this work afforded valuable insights into the PPCS enzyme, as well as the potential of HoPan and compounds that share its MOA to serve as leads in our on-going efforts to develop new selective CoA-targeting antimicrobial agents.

RESULTS AND DISCUSSION

Evaluating the interaction of HoPan with PanK: inhibitor, or substrate?

All previous studies that evaluated the impact of HoPan on the activity of the PanK enzymes of target organisms of interest were executed using discontinuous assays that rely on the turnover of radioactive substrates (either radiolabeled Pan or ATP). More specifically, it was shown that HoPan is an apparent competitive inhibitor of all mouse PanK isoforms when using [^{13}C]Pan as substrate and tracking the formation of the radiolabeled 4′-phosphopantothenate (P-Pan) product.[13] However, such an assay cannot distinguish between compounds acting as classical competitive *inhibitors* on the one hand, or as competitive *substrates* on the other (Figure 2A). In the latter case, the observed reduction in the rate of P-Pan formation would be due to HoPan also being turned over; the observed "K_i" would be the PanK enzyme's K_M for HoPan. Since the same study showed that murine hepatocytes can transform HoPan into P-HoPan, we hypothesized that it was more likely that HoPan's apparent inhibition of PanK's Pan phosphorylation activity was due to it acting as a competing substrate of the enzyme.

To establish whether HoPan's interaction with eukaryotic PanKs is that of a substrate or inhibitor, we prepared heterologously expressed and purified human and fruit fly PanKs to be used in *in vitro* activity assays. For these tests we used the two main cytosolic isoforms of human PanK (hPANK1β and hPANK3) and the Fumble D (FblD) splicing variant of the single fruit fly PanK (dPANK), which represents the minimally catalytically active form of the enzyme in this organism.[22] Importantly, the key catalytic and other sequence motifs of eukaryotic PanKs are largely conserved, suggesting a similar active site architecture — and therefore substrate specificity profile — for these enzymes (Figure 2B and Supplementary Figure S1). For the activity determination a standard continuous kinase assay was used that couples the formation of ADP to the oxidation of NADH, the latter of which is followed spectrophotometrically (Figure 2A). As such, the assay is naïve of the substrate used, and can be applied to determine the activity of the enzyme towards any substrate, or even mixtures of competing substrates.

The results, shown in Figure 2C and summarized in Table 1, clearly indicate that HoPan is a substrate of all the tested PanKs, with specificity constants (k_{cat}/K_M) no more than two-fold lower than that observed for the natural substrate, Pan. This difference was mainly due to increased K_M-values; at saturating concentrations, the enzymes showed no distinction in the rate of turnover of the two compounds. Both hPANK3 and dPANK/FblD the enzymes showed a degree of cooperative behavior towards HoPan but not Pan (as evidenced by sigmoidal activity profiles that gave Hill coefficients of ~1.3–1.55 when fit to the Hill equation), suggesting potential differences in the binding modes of the two substrates to the respective subunits of the PanK dimer.

An activity determination was also performed using the salvage metabolite PantSH as substrate (Figure 2C and Table 1). Interestingly, for both hPANK3 and dPANK/FblD the obtained k_{cat}/K_M values for PantSH were higher than those obtained for Pan, with dPANK/FblD showing full cooperativity and a 3-fold increase in its specificity constant (mainly due to a much-reduced $K_{0.5}$ value, the equivalent of the K_M value in a cooperative enzyme). This suggested that in its case, PantSH would be the preferred substrate in mixtures containing similar concentrations of Pan and/or HoPan.

HoPan, once metabolically activated by PanK, inhibits PPCS.

With the knowledge that eukaryotic PanKs accept HoPan as a substrate and convert it into P-HoPan, we set out to determine if this phosphorylated form inhibits or otherwise interacts with the next enzyme in the CoA pathway (PPCS), as was found to be the case for the natural product CJ-15,801 (also a Pan analogue) in *S. aureus*.[24] For these experiments, P-HoPan was chemically synthesized and its impact tested on the activity of heterologously expressed and purified human and fruit fly PPCS enzymes (otherwise known as CoaB proteins). The PPCS reaction takes place in two steps: in the first P-Pan's carboxylic acid group is activated with ATP to form an acyl adenylate (P-Pan-AMP, **8**) and pyrophosphate, while in the second step the activated acyl group is transferred to cysteine's amine to form 4′-phosphopantothenoylcysteine (P-PanCys, **5**), with the concomitant release of AMP (Figure 3A). For these tests we tracked the reaction progress in the absence and presence of increasing concentrations of P-HoPan using an assay that couples pyrophosphate formation to the oxidation of NADH.

The results clearly show that increasing amounts of P-HoPan reduces the rate of catalysis of both human (hPPCS) (Figure 3B) and fruit fly (dPPCS) (Figure 3C) enzymes. By plotting the fractional activity obtained at each inhibitor concentration an IC_{50} value can be obtained; having confirmed that the inhibition is indeed competitive towards P-Pan (Supplementary Figure S2), these values were converted to K_i values using the Cheng-Prusoff equation for competitive inhibitors (Eqn. 4).[25] The analysis was performed twice for each enzyme using different batches of enzymes in each case, giving an average K_i value of 13.4 ± 3.6 μM for hPPCS and 20.9 ± 1.1 μM for dPPCS (ave ± range/2), respectively. This indicates that, once formed, P-HoPan is a moderately potent competitive inhibitor of these enzymes.

Co-crystallization with P-HoPan and AMPPNP captures hPPCS in a fully ordered conformation.

The discovery of P-HoPan's inhibition of PPCS raises the question of the molecular mechanism by which this inhibition is achieved, considering the close structural similarity between P-HoPan and the P-Pan substrate. Unfortunately, none of the available PPCS structures could provide any insight in this regard due to a lack of appropriate complex structures, and because in all these structures several portions of the active site remained disordered. In the case of hPPCS only the *apo* structure has been determined, with large portions of the active site region found in a disordered state (PDB: 1P9O).[26] While X-ray structures of a site-directed mutant of the *Saccharomyces cerevisiae* PPCS (Cab2) revealed the binding mode of the P-Pan substrate (PDB: 6AI9), the intermediate P-Pan-CMP (PDB: 6AIK) and the P-PanCys product (PDB: 6AIM),[27] no structures were obtained in complex with the unreacted P-Pan substrate in the presence of nucleotide. Similarly, none of the available structures of bacterial PPCS enzymes—those of the *Escherichia coli* PPCS (*ec*PPCS)[28] and the *Mycobacterium smegmatis* CoaBC (bifunctional PPCS/PPCDC fusion)[29]—could shed light on a possible inhibition mechanism for P-HoPan.

We therefore determined the X-ray structure of hPPCS in complex with P-HoPan and the non-hydrolysable ATP analogue AMPPNP to a resolution of 1.9 Å (Supplementary Table S1). The final structure was a functional dimer (Figures 4A), with electron densities for the co-factor AMPPNP and the ligand P-HoPan observed in both monomers (Figure 4B). Both the ligands were found to be positioned perpendicular to each other (Figure 4B), a reaction geometry reminiscent of aminoacyl-tRNA (aa-tRNA) synthetases (Supplementary Figure S3).[30] This suggests that although the folds are evolutionarily diverse, the reaction mechanisms of both types of enzymes are very closely related. Importantly, the obtained structure is the first of any PPCS where all the active site loops as well as the *N*-terminal regions were completely ordered (Figures 4A, 4C & 4D). This allows for several important structural insights to be gained.

Specifically, the conformation of the dimerization loop (loop1, residues A188−A201) was well-defined in the ternary complex of hPPCS (Figures 4A & 4C). This loop crosses over to the other monomer and completes the active site of the adjacent subunit, acting as a lid that covers the solvent accessible nucleotide binding pocket (Figure 4A). The active site pocket that harbours ATP and the other substrates is sandwiched between helices α7 and α2 and by strand β7 (topology numbering is in accordance with *apo* hPPCS[26]) (Figure 4D). Like the bacterial and yeast PPCSs, one side of the nucleotide pocket is composed of mostly charged residues (contributed by both the subunits) that stabilize the tri-phosphate group of AMPPNP, while the other side adopts a shape that complements its adenine moiety (Figure 4D). In particular, the highly conserved residues K212, K231, L232, and E233 of one monomer, and K195 □ and S198 □ from the dimerization loop-1 of the other monomer, anchor the phosphate ions of AMPPNP. The ribose and adenine moieties are stabilized by the hydrogen and hydrophobic interactions with F230, A179, P211, L213, L159, V181, and V210 residues (Figure 4D). Further stabilization of the nucleotide is achieved via interaction with a Mg^{2+} ion that coordinates with the oxygen atoms of the AMPPNP phosphates, with two water molecules and with D183 (a conserved residue in all species). To ensure proper orientation of D183, R55 □ interacts from the neighbouring dimerization loop-2 (Figure 4D).

A loop at the N-terminus (residue 5–17) also adopted an ordered conformation in the ternary hPPCS complex (Figures 4A & 4E). Comparison with bacterial type-I PPCS enzymes shows that upon ligand and cofactor binding this loop anchors PPCDC (the next enzyme in the *de novo* pathway) for catalysis. Overall, the features of the solved ternary structure demonstrate that co-crystallization of hPPCS with P-HoPan and AMPPNP allowed us to capture the enzyme in a fully ordered/closed conformation. This provides the first information on the basis for P-HoPan’s inhibition mechanism.

P-HoPan binding leads to a non-reactive complex that traps hPPCS in a 'pre-catalytic' state.

The highly ordered nature of the hPPCS–P-HoPan–AMPPNP ternary complex suggested that P-HoPan interacts with the enzyme differently than its substrate, P-Pan. Analyzing the P-HoPan binding mode, we find that the phosphate and hydroxyl groups of P-HoPan are stabilized by the residues S61, S62 G63, R65, and N258 which is present on a loop near the N-terminus between α2 and β7 (Figure 4D). P-HoPan is also covered by a flexible flap (ligand capping loop) that creates a hydrophobic core for the stabilization of the 4′-phosphopantoyl moiety. This flap is comprised of seven residues (259−265) that were found to be disordered in the *apo* state, only achieving a well-defined conformation upon P-HoPan binding to hPPCS (Figure 4D & Figure 5A). While this flap is a common feature in all PPCS enzymes, it is longer (13 residues) in prokaryotes than in eukaryotes, forming a more compact pocket in the latter (Figure 5B). Importantly, P-HoPan's carboxylate group, which is the potential site of reaction, is anchored by a hydrogen bonding interaction with the backbone amide of both A180 and V181. These residues form part of the 'AAV(A/S)D' motif present at the C-terminus of β6, which is conserved in all PPCS enzymes (Figure 5C). This anchoring interaction is the key to explaining why P-HoPan acts as an inhibitor rather than a substrate of PPCS.

Comparison of the ternary complex of hPPCS with the structures of the yeast PPCS homologue Cab2 with P-Pan as well with its intermediates bound shows that, with respect to the β- and γ-phosphates of the nucleotide, P-Pan's carboxylate is positioned in an orientation that is ideal for nucleophilic attack at the α-phosphate, which will allow formation of the P-Pan-AMP intermediate (Figure 5D). In contrast, the carboxylate group of P-HoPan, due to the presence of the extra $-CH_2-$ group and the anchoring interaction, is positioned in an opposite conformation (Figure 5E). Consequently, the P-HoPan carboxylate cannot perform the nucleophilic attack on the α-phosphate of ATP to form the analogous P-HoPan-AMP intermediate; such an attack becomes conformationally too difficult to achieve within the constraints of the enzyme's active site architecture. Consequently, a stable non-reactive complex is formed, trapping the enzyme in a 'pre-catalytic' state and leading to the observed inhibition of PPCS activity. P-HoPan therefore inhibits PPCS by a new mechanism that may hold potential for the discovery of inhibitors of other therapeutically relevant ligases.

P-HoPan bound structure provides insight into cysteine binding and the PPCS catalytic mechanism, and allows for mapping of deleterious mutations.

The ternary complex of hPPCS allowed us to model the cysteine binding site, an important pre-requisite for proposing a catalytic mechanism of this enzyme. Previous reports have stressed that the enzyme uses a ping-pong mechanism to catalyse the conversion of P-Pan into P-PanCys, i.e. cysteine enters the active site only after formation of the acyl-cytidylate/adenylate intermediate.[26,28] However, the exact location of the cysteine binding site remained elusive.

To delineate the cysteine site we overlayed the co-ordinates of the intermediate conformation from the P-Pan-CMP bound Cab2 structure with that of the hPPCS ternary complex. This allowed for the intermediate-bound state of hPPCS to be recreated. When cysteine was docked using this structure as a template, its conformation was predominantly stabilized by residues inside a pocket that is lined by the conserved ‘AAV(A/S)D’ motif (Figure 5C & 5F). The stabilizing interactions included hydrogen bonding interactions with the conserved residues T41 (at β1-strand), A178 and A179 (at a hydrophobic loop) and Y155 (at helix α5). Based on previously performed mutagenesis and HPLC-based assays on *E. coli* PPCS, it has been proposed that residues A178 and A179 of the conserved ‘AAV(A/S)D’ motif (Figure 5C) participate in the final step of the reaction, i.e. the attack of cysteine on the reaction intermediate to form PPC.[28] Moreover, the $–NH_2$ group of the modelled cysteine is properly positioned for this nucleophilic attack, pointing directly towards the carbonyl group of the intermediate (Figure 5F). We therefore believe that the modelled conformation of cysteine is a true representation of its occupancy inside the pocket. However, our model is in contrast to the mechanism proposed for Cab2, which suggests that the cysteine binds inside the pocket via interaction with K195 □ and K231 (K226 □ and K281 in Cab2 PPCS).[27] We believe that such a conformation is not conducive to formation of the amide bond as attack of the amine on the carbonyl group from the front side would be sterically unfavorable (Figure 5F). Based on the proposed cysteine binding site, we developed a proposal for the PPCS catalytic mechanism that is supported by the currently available structure data (Supplementary Figure S4).

Finally, the obtained hPPCS ternary structure also allows for the mapping of two mutations and a deletion (A180P, E233V and Δ107−111) in hPPCS that have been linked to severe dilated cardiomyopathy.[32] Of these, the A180P and E233V mutations were categorized as highly deleterious, but the previously available *apo* structure of hPPCS (PDB: 1P9O) with its largely disordered active site did not provide insight into the functional relevance of these mutants. A description of the location and functional implication of these mutants is provided in the Supporting Information, and in Supplementary Figure S5.

Validating HoPan’s proposed molecular mechanism of action in S2 insect cells.

We next turned to validating the molecular MOA revealed for HoPan in a whole cell model. This was done using *D. melanogaster* Schneider’s cells (S2 cells), as these have been used extensively for studying CoA levels and their relationship to neurodegenerative phenotypes, and since the levels of dPANK/Fbl and dPPCS can be modulated in these cells using RNA interference (RNAi)-mediated down-regulation, or by overexpression.[14,15,33–35] Importantly, the S2 cells are also sensitive to HoPan treatment.

The conclusion drawn from the *in vitro* data—that P-HoPan inhibits PPCS—predicts that P-PantSH will rescue a HoPan induced phenotype, but that P-Pan (downstream from dPANK/Fbl but upstream from PPCS) will not (Figure 1). First, we determined whether P-Pan is taken up by S2 cells. RNAi was used to generate dPANK/Fbl depleted S2 cells. Consistent with previous reports,[14,15,34] dPANK/Fbl-depleted cells show a decreased cell count and decreased histone-acetylation levels (Figures 6A, 6B and Supplementary Figure S6A). This phenotype is rescued by addition of either P-PantSH[15] or P-Pan (Figure 6A), indicating that both compounds enter S2 cells to enable continuation of CoA biosynthesis in the absence of dPANK activity.

Next, S2 cells were treated with 1 mM HoPan, which is known to reduce cell count and histone acetylation.[14,15] While addition of 100 μM P-PantSH nearly completely reversed the impact of HoPan inhibition on cell count (Figure 6C) and histone acetylation (Figure 6D & Supplementary Figure S6B), P-Pan was not able to show significant rescue as it did in the RNAi experiment, with only a small effect at a high concentration (300 μM). These results are consistent with an inhibitory action of P-HoPan on PPCS. Moreover, overexpression of dPANK/Fbl also did not result in any significant rescue of the cell count (Figure 6E) and histone acetylation (Figure 6F & Supplementary Figure S6C) phenotypes in S2 cells treated with increasing concentrations (up to 2.0 mM) of HoPan. In contrast, overexpression of dPPCS did show some rescue of the cell count (Figure 6E), and histone acetylation was significantly improved compared to the control (GFP overexpression) (Figure 6F & Supplementary Figure S6C). Taken together, these results support the conclusion that the molecular target of HoPan is PPCS, and not PanK as has previously been asserted.

CONCLUSIONS

The pantothenate analogue HoPan is a well-known modulator of CoA levels in various systems and disease models that was thought to act by inhibiting PanK, the first enzyme of CoA biosynthesis. This study shows that PanK in fact serves as metabolic activator of HoPan, phosphorylating it and turning it into an inhibitor of the next CoA biosynthetic enzyme, PPCS. This molecular MOA explains why PanK was previously considered to be HoPan’s target: by acting as an alternative substrate of PanK, it competes with Pan (the enzyme’s natural substrate) for PanK-mediated phosphoryl transfer, thereby effectively reducing the rate of P-Pan formation. In this manner the negative impact on CoA biosynthesis is compounded: first by reducing the rate of P-Pan formation (albeit transiently, i.e. as long as unphosphorylated HoPan is present), and second by inhibiting PPCS. It is likely that the HoPan-induced phenotypes are a result of this combinatorial inhibition of CoA biosynthesis, as the determined K_i values for P-HoPan’s inhibition of PPCS alone is relatively modest.

Due to its dependence on PanK for metabolic activation, and its competition with Pan for this transformation, HoPan’s effective potency is expected to be highly dependent on the amount of Pan present in the environment. Indeed, the conflicting reports on HoPan’s toxicity in various animals and humans can be reconciled with a knowledge of the circulating levels of Pan in each case, and/or whether Pan was withheld from or added to the diet.[12,13,36,37] Consequently, contrary to the conclusion of some of these early studies that HoPan induces a Pan deficiency, it is more likely that an underlying Pan deficiency resulted in an apparent increase in HoPan’s potency. One could therefore reasonably conclude that HoPan may be potent inhibitor under conditions where Pan availability is limited. For example, plants rely on their own *de novo* biosynthesis of Pan, and HoPan treatment of cucumber, tomato, rice and maize was found to suppress root and shoot growth, and at higher concentrations also decreased seed germination.[38] On the other hand, as Pan availability does not limit CoA synthesis in the heart one would predict that HoPan would not show the same cardiac effects as those associated with the PPCS mutations in humans.[39]

Our results show that the inhibitory potential of HoPan—and any other inhibitor with a similar MOA—can be predicted by considering four factors: first, the potency of the metabolically activated inhibitor acting on PPCS *in vitro*; second, the concentration levels of Pan in the environment where inhibition is to occur; third, the specific activity of PanK enzyme toward the inhibitor compared to Pan; and fourth, the availability of mechanisms to bypass PPCS inhibition, e.g. a functional CoA salvage pathway (Figure 1). These factors and their interplay provide a framework for directing the rational development of inhibitors and modulators of CoA biosynthesis. This will be aided by the co-structure obtained in this study that uncovered previously unknown details about the mechanism of PPCS enzymes—including important insights into its elusive cysteine binding mechanism.

Taken together, the molecular MOA elucidated for HoPan here indicates that the underlying basis for the phenotypes it induces is more complex than originally thought. Moreover, our study significantly advances our understanding of small molecule inhibitors of CoA biosynthesis, of the diversity in the mechanisms by which they exert an effect on the pathway, and of the mechanistic and kinetic characteristics of PanK and PPCS—two CoA pathway enzymes that are associated with human genetic diseases and that are also targeted for the development of new antimicrobial drugs. These insights are likely to prove highly valuable in our search for new therapies in these areas.

METHODS

General materials and methods.

Unless otherwise stated, all chemicals and reagents where from Merck-Millipore/Sigma-Aldrich. All NMR analyses were performed using 300 MHz Varian VNMRS, 400 MHz Varian Unity Inova or 600 MHz Varian Unity Inova instruments at the Central Analytical Facility (CAF) of the University of Stellenbosch. Chemical shifts (δ) are given in ppm, with the abbreviations indicating multiplicity (s = singlet, t = triplet, q = quartet, m = multiplet), coupling constant (J) in Hz, and integration of the observed signals. All restriction enzymes were purchased from New England Biolabs or Thermo Scientific (FastDigest).

P-HoPan synthesis.

Phospho-hopantenate (P-HoPan) was synthesized by adaptation of the method used to synthesize P-Pan.[40] Sodium γ-aminobutyrate (694 mg, 4.85 mmol) was combined with pantolactone (694 mg, 5.33 mmol) and heated overnight at 140°C before being lyophilized. The reaction mixture was subsequently dissolved in 5 mL distilled water passed through an Amberlite® (IR120 H^+ form) column (0.6 g). The collect product solution was dried by lyophilization, and purified by flash column chromatography (Merck silica gel 60, particle size 0.040–0.063 mm; ethyl acetate/methanol/acetonitrile/distilled water 5:2:1:1) to give HoPan as a yellow oil (888 mg, 3.8 mmol, yield 78%). HoPan was combined with an equivalent of NaOH (1 M solution) and dried by lyophilization before being dissolved in 15 mL dry *N*,*N*-dimethylformamide (DMF) and esterified with benzyl bromide (471 μL, 3.97 mmol) by heating the mixture at 70°C overnight while stirring. The solvent volume was reduced *in vacuo* and the product dissolved in 100 mL ethyl acetate, followed by washing of the organic layer with saturated aqueous NaCl (3×20 mL). The organic phase was dried over anhydrous Na_2SO_4, filtered and the solvent removed *in vacuo*. The product was purified by flash column chromatography (Merck silica gel 60, particle size 0.040–0.063 mm; ethyl acetate/hexane 3:1 to 5:1) yielding the intermediate (HoPan benzyl ester) as a clear oil (311 mg, 0.96 mmol, yield 25%). ^1H NMR (300 MHz, $CDCL_3$): δ 0.91 (s, 3H), 1.02 (s, 3H), 1.84–1.94 (m, 2H), 2.43 (t, *J*=7.2 Hz, 2H), 3.30–3.38 (m, 2H), 3.50 (q, *J*=16.3 Hz, 2H), 4.00 (s, 1H), 5.12 (s, 2H), 7.36 (arom, 5H). Dibenzylchlorophosphate was subsequently prepared by stirring dibenzylphosphite (756 mg, 2.9 mmol) and *N*-chlorosuccinimide (385 mg, 2.9 mmol) in dry toluene (3.85 ml) for 2 hours at room temperature. The succinimide was removed by filtration and the filtrate added dropwise to a solution of HoPan benzyl ester (311 mg, 0.96 mmol) dissolved in dry pyridine (4.33 mL). The mixture was stirred at –40°C (in a dry ice/acetonitirile bath) for 2 hours and placed in a –20°C freezer overnight. After warming to room temperature, the reaction mixture was quenched with 1.44 mL distilled water before removal of the solvent *in vacuo*. Ethyl acetate (50 mL) was added, after which the organic layer was washed with 1 M H_2SO_4 (2×10 mL) and 1 M $NaHCO_3$ (2×10 ml), followed by drying over anhydrous Na_2SO_4. The mixture was filtered and the solvent removed *in vacuo*, after which the crude product was purified by flash column chromatography (Merck silica gel 60, particle size 0.040–0.063 mm; ethyl acetate/hexane 4:1) to give HoPan benzyl ester dibenzylphosphate as a colourless oil (127 mg, 0.22 mmol, yield 23%). ^1H NMR (400 MHz, $CDCl_3$): δ 0.80 (s, 3H), 1.09 (s, 3H), 1.84–1.92 (m, 2H), 2.42 (t, *J*=7.4 Hz, 2H), 3.31 (q, *J*=13.3 Hz, 2H), 3.52 (t, *J*=9.8 Hz, 1H), 3.92 (s, 1H), 4.06 (q, *J*=10.2 Hz, 1H), 5.00–5.10 (m, 4H), 5.13 (s, 2H),7.36 (arom, 15H). The removal of the benzyl protecting groups was performed by dissolving the compound in a 9:1 mixture of methanol and water (10 mL), followed by the addition of Pd/C catalyst (34.7 mg, 0.33 mmol). The mixture was stirred for 3 hours under an H_2 atmosphere (H_2-filled balloon). The progress of the reaction was monitored by thin layer chromatography (TLC; aluminium-backed Merck silica gel 60 F254 plates; visualized by UV and by application of a cerium ammonium molybdate (CAM) stain). Upon completion of the reaction, the mixture was filtered, and the solvent reduced *in vacuo*. The product was lyophilized to yield P-HoPan as a clear oil (45 mg, 0.14 mmol, 64% yield). The product was dissolved in distilled water, titrated to pH 6.5 with 1 M NaOH and stored as a stock solution (100 mM) at −20°C. ^1H NMR (300 MHz, D_2O): δ 0.81 (s, 3H), 0.88 (s, 3H), 1.67–1.77 (m, 2H), 2.32 (t, *J*=7.5 Hz, 2H), 3.17 (t, *J*=6.9 Hz, 2H), 3.53 (q, *J*=9.8 Hz, 1H), 3.73 (q, *J*=9.68 Hz, 1H), 3.93 (s, 1H). ^{13}C NMR (75 MHz, D_2O): δ 19.46, 21.35, 24.61, 30.16, 31.85, 38.81, 39.04, 175.58, 178.67, 236.52. ^{31}P NMR (300 MHz, D_2O) δ 0.94 (s, 1P).

Plasmids and constructs.

To obtain expression plasmids for hPANK1β and hPANK3, the gene sequences were optimized for expression in *E. coli*, synthesized and provided in pUC vectors flanked by appropriate restriction enzyme cleavage sites by GenScript USA Inc. The sequence encoding hPANK1β (UniProt/Q8TE04.2) was subcloned into the pET20b expression vector using the NdeI and XhoI restriction sites respectively, yielding the plasmid pET20b-HsPANK1β. The sequence encoding residues 12–398 of hPANK3 (UniProt/Q9H999.1), together with an N-terminal 6×His-tag and thrombin cleavage site, was subcloned into the pET28a expression vector using the NcoI and XhoI restriction sites to give the plasmid pET28a-HsPANK3. The plasmid pET28a-dPANK/FblD expressing dPANK/FblD (UniProt/Q9NHN2; residues 112–

512) with both N- and C-terminal 6×His-tags was amplified by PCR from S2 cDNA and inserted into the pET28a expression vector using the NdeI and EcoRI restriction sites. The gene encoding dPPCS (UniProt/Q7KN99) was subcloned from pAc PPCS into the pET28a expression vector using the NheI and EcoRI restriction sites, yielding the plasmid pET28a-dPPCS encoding dPPCS with an N-terminal 6×His-tag and thrombin cleavage site. The plasmid pPROEx-hPPCS encoding hPPCS (UniProt/Q9HAB8) was previously prepared,[41] and was a kind gift from Andrei Osterman. The plasmids pAc dPANK/FblE and pAc dPPCS were created by amplifying the respective genes by PCR from S2 cDNA and inserting them in the plasmid pAc 5.1 (Invitrogen) with EcoRI and XbaI or EcoRI and KpnI. Plasmid pAc GFP was created by amplifying the GFP-encoding gene by PCR from pEGFP-C1 (Clontech) and inserting it in pAc 5.1 with AgeI and BbstBI.

Expression and purification of enzymes for kinetic assays.

hPPCS was expressed and purified as previously reported.[26,41] hPANK3, dPANK/FblD and dPPCS were expressed in *E. coli* BL21(DE3), while hPANK1β was expressed in *E. coli* C41(DE3) + pLysS. A starter culture was made by adding a single colony from plate of the expression host transformed with the required plasmid, and grown overnight at 37°C. For batch expression, 500 mL of LB media was inoculated with 5 mL starter culture, and grown at 37°C while shaking at 180 rpm. When the required density was reached (OD_{600} of 0.6 for dPPCS, and 0.9 for the other enzymes), expression was induced by addition of isopropyl-β-D-thiogalactopyranoside (IPTG). For dPPCS, 0.1 mM IPTG was used and expression was allowed to occur overnight at 37°C. For hPANK1β, hPANK3 and dPANK/FblD 1 mM IPTG was used, followed by overnight expression at 18°C. Cultures were collected by centrifugation and pellets were stored at −20 °C until purification. Pellets were resuspended and sonicated on ice in 25 mL sonication buffer (25 mM Tris-HCl pH 7.9, 300 mM NaCl, 10 mM imidazole, 0.033% Brij-35, 5% glycerol) containing 2 mM PMSF, half a protease inhibitor cocktail tablet (COmplete EDTA free, Roche) and 17.5 μL 2-mercaptoethanol. After sonication, the samples were centrifuged for 20 minutes at 75 600×g and the lysates were subjected to immobilized nickel affinity chromatography on an ÄKTAprime protein purification system. Non-specific proteins bound to the resin were washed with 75 mM imidazole in binding buffer (25 mM Tris-HCl pH 7.9, 300 mM NaCl, 5 mM imidazole) followed by elution of the target protein with 500 mM imidazole in binding buffer. Fractions containing the target protein were pooled and subjected to buffer exchange, replacing the elution buffer with storage buffer (20 mM Tris-HCl pH 8.0, 5 mM $MgCl_2$). Purified protein fractions were aliquoted, flash frozen in liquid nitrogen and stored at –80°C. The concentration of each enzyme was determined with the Bradford method and a BSA standard using the Rapid protein quantification kit from BioRad. The purity of the enzymes was confirmed by 12% SDS-PAGE analysis.

PanK assay and data analysis.

PanK activity was determined using a previously described continuous PK/LDH enzyme-coupled spectrophotometric assay[20] that couples the production of ADP to the oxidation of NADH. An extinction coefficient of 6220 $M^{-1}.cm^{-1}$ was used for NADH. All assays with hPanK1β and hPANK3 were performed at 25°C in clear, flat bottom 96-well plates (Greiner Bio-One), with each reaction performed in triplicate at a final volume of 300 μL.

Each 300 μL reaction mixture contained 50 mM Tris-HCl (pH 7.6), 10 mM $MgCl_2$, 20 mM KCl, 0.5 mM NADH, 2 mM phosphoenolpyruvate, 1.5 mM ATP, 0.01 U.μL^{-1} PK, 0.01 U.μL^{-1} LDH and 16.7 ng.μL^{-1} PanK. The reactions were initiated by the addition of Pan (3.125–200 μM) and was monitored for 5 min at 6 second intervals by a Varioskan multimode plate reader (Thermo Scientific). When PantSH was tested as substrate, 0.2 mM of tris(2-carboxyethyl)phosphine (TCEP) was added to the reaction mixture to reduce the disulfide. For dPANK/FblD, initial assays were performed under the same conditions as for the human PanKs, except at a Pan concentration range of 6.25–400 μM and at a final reaction volume of 150 μL. Due to the low expression yield of this enzyme, subsequent assays were performed in clear, flat bottom 384-well plates (Greiner Bio-One) using a total reaction volume of 50 μL on a Varioskan Flash multimode plate reader (Thermo Scientific). For each assay, kinetic profiles were obtained by determining initial rates at each substrate concentration in triplicate. The kinetic parameters of interest were determined by fitting either the Michaelis-Menten equation (Eqn. 1) or the Hill-equation (Eqn. 2) (see Table 1) using SigmaPlot 14.0 (Systat Software, Inc.) to the data. The kinetic parameters reported in Table 1 are the average of those determined for the indicated number of experiments, each performed with a different batch of enzyme.

$$\boldsymbol{v} = \frac{\boldsymbol{V_{max}} \times [\mathrm{S}]}{\boldsymbol{K}_{\mathrm{M}} + [\mathrm{S}]} \qquad \text{Eqn. 1}$$

$$\boldsymbol{v} = \frac{\boldsymbol{V_{max}} \times [\mathrm{S}]^{\boldsymbol{h}}}{\boldsymbol{K}_{0.5} + [\mathrm{S}]^{\boldsymbol{h}}} \qquad \text{Eqn. 2}$$

PPCS assay and data analysis.

PPCS assays were performed as previously described[24] using a continuous enzyme coupled assay kit (Pyrophosphate reagent, Merck-Millipore/Sigma-Aldrich cat. # P7275) that couples the formation of pyrophosphate by PPCS to the oxidation of NADH. An extinction coefficient of 6220 $M^{-1}.cm^{-1}$ was used for NADH. Assays were performed at 37°C in clear, flat bottom 96-well plates (Greiner Bio-One), with each reaction performed in duplicate at a final volume of 100 μL. Each 100 μL reaction contained PPCS enzyme (200 nM hPPCS or 100 nM dPPCS respectively), 1 mM ATP, 1 mM L-cysteine, 2.5 mM TCEP, 50 mM Tris-HCl (pH 7.6), 20 mM KCl, 10 mM $MgCl_2$ and 40 μL pyrophosphate reagent (each vial was dissolved in 4.5 mL distilled H_2O). Reactions were initiated with 150 μM P-Pan[40] and P-HoPan (at a range of 12.5–400 μM) and the oxidation of NADH was continuously measured with a Multiskan Sky microplate spectrophotometer (Thermo Scientific) at 340 nm at 10 second intervals over 15 minutes. Pyrophosphate formation was plotted as progress curves and the fractional activities for each duplicate reaction were calculated. These fractional activities were plotted and an IC_{50} was calculated in SigmaPlot 14.0 (Systat Software, Inc.) using Eqn. 3. Each IC_{50} value was converted to a K_i value, using the Cheng-Prusoff equation for competitive inhibitors (Eqn. 4). For each enzyme two K_i values were determined from two independent experiments using two different enzyme batches; the reported value is the average K_i value that was obtained.

$$\frac{\boldsymbol{v_i}}{\boldsymbol{v}_0} = \frac{1}{1 + \frac{[\mathrm{I}]}{\mathrm{IC}_{50}}} \qquad \text{Eqn. 3}$$

$$\boldsymbol{K_i} = \frac{\mathrm{IC}_{50}}{1 + \frac{[\mathrm{S}]}{\boldsymbol{K}_{\mathrm{M}}}} \qquad \text{Eqn. 4}$$

hPPCS purification for crystallization.

The hPPCS protein used for crystallization and structure determination was obtained using previously reported methods.[26] In brief, the starter culture was made by adding a single colony from transformed plate, grown overnight at 37°C, in 10 mL of LB media containing 50 mg/mL of ampicillin. 5 L of LB media was inoculated with 50 mL of saturated starter culture and incubated at 37°C. When the culture reached an OD of approx. 0.6, the temperature was lowered to 16°C, and cells were induced with 0.1 mM IPTG for 16 hrs. Cells were harvested by centrifugation at 4 500 rpm for 20 mins, and the cell pellet was re-suspended in 30 mL ice-cold lysis buffer (50 mM Tris-HCl pH 8.0, 500 mM NaCl, 5 mM imidazole). Cells were lysed by sonication and cell debris was removed by centrifugation at 18 500×g for 45 minutes. The supernatant of protein solution was mixed with 500 μL of a slurry of Ni-nitrilotriacetic acid resin (Qiagen) pre-equilibrated in lysis buffer, followed by incubation for 2 hrs. The supernatant was separated by centrifugation at 250×g for 25 mins. Non-specifically bound proteins were removed by extensive washing with wash buffer (50 mM Tris-HCl pH 8.0, 500 mM NaCl, 30 mM imidazole). The His-tagged protein was eluted with the elution buffer (50 mM Tris-HCl pH 8.0, 500 mM NaCl) using a gradient of imidazole from 60 to 300 mM. The purity of the protein in the collected fractions was verified by 15% SDS-PAGE analysis. Fractions containing pure protein were pooled, desalted in dialysis buffer (50 mM Tris-HCl pH 8.0) and concentrated to a final concentration of 500 μM.

Crystallization, data collection and refinement.

The initial crystallization condition for the protein was determined from the matrix screen provided by Hampton research (crystal screen 1 and crystal screen 2). 300 μM protein was pre-incubated with 5 mM AMPPNP, 5 mM P-HoPan and 10 mM $MgCl_2$. Crystals were grown at 18°C by hanging drop vapor diffusion method. Diffraction quality crystals grew within 4 weeks in 0.2 M lithium sulfate monohydrate, 0.1 M Tris HCl and 30% PEG 4000 in the drop size of 6 μL having 2:1 ratio of protein mixture and reservoir solution, respectively. A single wavelength data set was collected at the beamline ID23 at European synchrotron radiation facility (ESRF), Grenoble, France. Before data collections, crystal was incubated in the cryo-protectant prepared by adding 20% glycerol in reservoir solution to prevent crystal damage from continuous X-ray exposure. 1600 frames were collected with 0.5 sec exposure time using PILATUS detector. Frames were indexed, integrated and scaled at 1.9 Å resolution in C2 space group using XDS software.[42] Phases were generated and structure was determined by performing molecular replacement in Phaser[43] in CCP4i suite[44] against the published structure of apo hPPCS (PDB: 1P9O).[26] Structure models were subjected to rigid body refinement and further refined using several cycles in Refmac5[45] in CCP4i suite.[44] Manual model building was performed with WinCoot.[46,47] Crystallographic data statistics are reported in Supplementary Table S1. The structure coordinates are available from the PDB with ID 7EDZ.

Docking of cysteine binding pocket in hPPCS.

Docking studies were undertaken to model the cysteine binding site. The dimeric crystal structure of the ternary complex of hPPCS with P-HoPan and AMPPNP was used as a template. In line with previous proposals, the cysteine enters to the active pocket only after cytidylate or adenylate intermediate formation.[26,28] Therefore, to mimic the intermediate state of hPPCS, the co-ordinates of intermediate from the P-Pan-CMP bound Cab2 crystal structure (PDB: 6AIK) were probed into the active site of hPPCS.[27] Using this intermediate-bound hPPCS structure as a base, cysteine binding site was docked using AutoDock 2.0 software, employing a Lamarckian genetic algorithm and free energy scoring function.[48] AutoDock calculation includes following steps; 1) co-ordinate file preparation, 2) pre-calculation of atomic affinities using AutoGrid, 3) docking of ligand, and 4) analysis of results. The grid box was selected in the active site formed by the two monomers and rigid docking was carried out using 200 runs. Run 139 with the cluster rank 2 (having a maximum, i.e., 118 conformations in the cluster) and the lowest binding energy of −4.19 kcal/mol was chosen as the model.

Drosophila S2 cell culture, RNA interference, and P-Pan and P-PantSH treatment.

Drosophila Schneider’s S2 cells were maintained at 25°C in Schneider’s *Drosophila* medium (Invitrogen) supplemented with heat-inactived 10% fetal calf serum (FCS, Gibco) and antibiotics (penicillin-streptomycin; Invitrogen) under laboratory conditions. Cells in the exponential phase of growth were used for all the experiments. Synthesis of double-stranded RNA (dsRNA) and RNAi treatment were carried out as described previously.[14] Nonrelevant (human gene; hMAZ) dsRNA was used as a control. After incubating the cells for 3 days with dsRNA to induce efficient knockdown, cells were subcultured with or without P-Pan (varying concentrations) or 100 μM P-PantSH (Syncom, >94%) and maintained for an additional 4 days until analysis for rescue efficiency of the compounds. The stock solutions of compounds were made in sterile water and stored at −20°C until use.

HoPan treatment of *Drosophila* S2 cells in combination with P-Pan and P-PantSH treatment.

Drosophila Schneider’s S2 cells were maintained under standard conditions as described above. Different concentrations of P-Pan or 100 μM P-PantSH were added to S2 cells in either the presence or the absence of 1 mM HoPan (Zhou Fang Pharm Chemical; 99%) for 48 h. As readouts, analysis of cell count and histone acetylation was performed as explained below.

HoPan treatment of *Drosophila* S2 cells overexpressing Fbl or PPCS.

Drosophila Schneider’s S2 cells were maintained under standard conditions as described above. S2 were seeded in Schneider’s Drosophila medium supplemented with heatinactivated 10% dialyzed serum (Fisher Scientific), and antibiotics (penicillin-streptomycin), transfected with the indicated plasmids using Effectene (Qiagen) according to the protocol of the manufacturer. After 24 hours HoPan was added in the different concentrations and incubated for another 48 hours. Cells were counted and analysed for histone acetylation as described below.

Western blotting analysis and antibodies.

For western blotting analysis, cells were collected, washed with PBS and centrifuged. The cells were lysed and sonicated in 1× Laemmli sample buffer and boiled for 5 min with 5% β-mercaptoethanol. Protein content was determined via DC protein assay (Bio-Rad). Equal amounts of protein were loaded on 10% or 12.5% mini protean TGX stain-free gels (Bio-Rad), transferred onto PVDF membranes using the Trans Blot Turbo System (Bio-Rad). Blocked with 5% fat free milk in PBS + 0.1% Tween for 1 hour at room temperature, after which they were incubated overnight with primary antibodies at 4°C. The primary antibodies used were rabbit anti-dPANK/Fbl (1:4,000, Eurogentec, custom made[33]), rabbit anti-dPPCS (1:4,000, Eurogentec, custom made[33]), mouse anti-tubulin (1:5,000, Sigma-Aldrich, T5168) and anti–acetyl-Histone (1:2,000, Active Motif, 39139[49]). Appropriate horseradish peroxidase–conjugated secondary antibodies (Amersham) were used and incubation occurred for 1.5 hours at room temperature. Membranes were developed using ECL reagent (Thermo Fisher Scientific) and the signal was visualized using the ChemiDoc imager (Bio-Rad), images exported as .tiff files and densitometric analysis of band intensities was performed using Image Studio Lite (Li-Cor).

Supplementary Material

Refer to Web version on PubMed Central for supplementary material.

ACKNOWLEDGMENTS

This project was funded by a grant from the National Research Foundation (NRF) of South Africa (grant # 93430) and NIH grant R01AI136836 to E.S., and by an Indo-South Africa Joint Science and Technology Research Cooperation Grant awarded to R.A. and E.S. by the Department of Science and Technology, Government of India (grant # DST/INT/SOUTH AFRICA/P-04/2014) and the NRF of South Africa (grant # 90702). K.J.M. was supported by an NRF Innovation Doctoral bursary from the NRF.

REFERENCES

(1). Strauss E (2010) Coenzyme A Biosynthesis and Enzymology, In Comprehensive Natural Products II Chemistry and Biology (Mander L, and Liu H-W, Eds.), pp 351–410, Elsevier, Oxford.

(2). Pietrocola F, Galluzzi L, Bravo-San Pedro, José M, Madeo F, and Kroemer G (2015) Acetyl Coenzyme A: A Central Metabolite and Second Messenger, Cell Metab. 21, 805–821. [PubMed: 26039447]

(3). Hayflick Susan J. (2014) Defective pantothenate metabolism and neurodegeneration, Biochem. Soc. Trans. 42, 1063–1068. [PubMed: 25110003]

(4). Jackowski S, and Leonardi R (2014) Deregulated coenzyme A, loss of metabolic flexibility and diabetes, Biochem. Soc. Trans. 42, 1118–1122. [PubMed: 25110012]

(5). Srinivasan B, and Sibon OCM (2014) Coenzyme A, more than 'just' a metabolic cofactor, Biochem. Soc. Trans. 42, 1075–1079. [PubMed: 25110005]

(6). Currais A, Huang L, Goldberg J, Petrascheck M, Ates G, Pinto-Duarte A, Shokhirev MN, Schubert D, and Maher P (2019) Elevating acetyl-CoA levels reduces aspects of brain aging, eLife 8, e47866. [PubMed: 31742554]

(7). Moolman WJ, de Villiers M, and Strauss E (2014) Recent advances in targeting coenzyme A biosynthesis and utilization for antimicrobial drug development, Biochem. Soc. Trans. 42, 1080–1086. [PubMed: 25110006]

(8). Jujo R (1944) Pantothenic acid and its allied compounds. II, Yakugaku Zasshi 64, 1.

(9). Nishizawa Y, Kodama T, Ishida R, Adachi S, and Kowa Y (1968) Homopantothenic acid. II. Electrophysiological investigations on homopantothenic acid, J. Vitaminol. 14, 345–353.

(10). Voronina TA, and Litvinova SA (2017) Pharmacological effects and clinical application of pantogam and pantogam active, Zh Nevrol. Psikhiatr. Im. S. S. Korsakova 117, 132–139.

(11). Rozanov VA (1979) Studies of the metabolism of GABA-^{14}C and pantoyl-GABA-^{14}C in mice, Ukr. Biokhim. Zh. 51, 629–633. [PubMed: 543029]

(12). Nishizawa Y, Kodama T, Noguchi Y, Nakayama Y, Hori M, and Kowa Y (1969) Homopantothenic acid. V. Chronic toxicity and teratogenic effect of homopantothenic acid, J. Vitaminol. 15, 26–32.

(13). Zhang Y-M, Chohnan S, Virga KG, Stevens RD, Ilkayeva OR, Wenner BR, Bain JR, Newgard CB, Lee RE, Rock CO, and Jackowski S (2007) Chemical Knockout of Pantothenate Kinase Reveals the Metabolic and Genetic Program Responsible for Hepatic Coenzyme A Homeostasis, Chem. Biol. 14, 291–302. [PubMed: 17379144]

(14). Siudeja K, Srinivasan B, Xu L, Rana A, de Jong J, Nollen EAA, Jackowski S, Sanford L, Hayflick S, and Sibon OCM (2011) Impaired Coenzyme A metabolism affects histone and tubulin acetylation in Drosophila and human cell models of pantothenate kinase associated neurodegeneration, EMBO Mol. Med. 3, 755–766. [PubMed: 21998097]

(15). Srinivasan B, Baratashvili M, van der Zwaag M, Kanon B, Colombelli C, Lambrechts RA, Schaap O, Nollen EA, Podgorsek A, Kosec G, Petkovic H, Hayflick S, Tiranti V, Reijngoud D-J, Grzeschik NA, and Sibon OCM (2015) Extracellular 4’-phosphopantetheine is a source for intracellular coenzyme A synthesis, Nat. Chem. Biol. 11, 784–792. [PubMed: 26322826]

(16). Leonardi R, Zhang Y-M, Yun M-K, Zhou R, Zeng F-Y, Lin W, Cui J, Chen T, Rock CO, White SW, and Jackowski S (2010) Modulation of Pantothenate Kinase 3 Activity by Small Molecules that Interact with the Substrate/Allosteric Regulatory Domain, Chem. Biol. 17, 892–902. [PubMed: 20797618]

(17). Di Meo I, Colombelli C, Srinivasan B, de Villiers M, Hamada J, Jeong SY, Fox R, Woltjer RL, Tepper PG, Lahaye LL, Rizzetto E, Harrs CH, de Boer T, van der Zwaag M, Jenko B, Cusak A, Pahor J, Kosec G, Grzeschik NA, Hayflick SJ, Tiranti V, and Sibon OCM (2017) Acetyl-4’-phosphopantetheine is stable in serum and prevents phenotypes induced by pantothenate kinase deficiency, Sci. Rep. 7, 1–12. [PubMed: 28127051]

(18). Virga KG, Zhang Y-M, Leonardi R, Ivey RA, Hevener K, Park H-W, Jackowski S, Rock CO, and Lee RE (2006) Structure-activity relationships and enzyme inhibition of pantothenamide-type pantothenate kinase inhibitors, Bioorg. Med. Chem. 14, 1007–1020. [PubMed: 16213731]

(19). Balibar CJ, Hollis-Symynkywicz MF, and Tao J (2011) Pantethine Rescues Phosphopantothenoylcysteine Synthetase and Phosphopantothenoylcysteine Decarboxylase Deficiency in *Escherichia coli* but Not in *Pseudomonas aeruginosa*, J. Bacteriol. 193, 3304–3312. [PubMed: 21551303]

(20). de Villiers M, Barnard L, Koekemoer L, Snoep JL, and Strauss E (2014) Variation in Pantothenate Kinase Type Determines Pantothenamide Mode of Action and Impacts on Coenzyme A Salvage Biosynthesis, FEBS J. 281, 4731–4753. [PubMed: 25156889]

(21). de Villiers M, Spry C, Macuamule CJ, Barnard L, Wells G, Saliba KJ, and Strauss E (2017) Antiplasmodial Mode of Action of Pantothenamides: Pantothenate Kinase Serves as a Metabolic Activator Not as a Target, ACS Infect. Dis. 3, 527–541. [PubMed: 28437604]

(22). Wu Z, Li C, Lv S, and Zhou B (2009) Pantothenate kinase-associated neurodegeneration: insights from a *Drosophila* model, Hum. Mol. Genet. 18, 3659–3672. [PubMed: 19602483]

(23). Subramanian C, Yun M-K, Yao J, Sharma LK, Lee RE, White SW, Jackowski S, and Rock CO (2016) Allosteric Regulation of Mammalian Pantothenate Kinase, J. Biol. Chem. 291, 22302–22314. [PubMed: 27555321]

(24). van der Westhuyzen R, Hammons JC, Meier JL, Dahesh S, Moolman WJ, Pelly SC, Nizet V, Burkart MD, and Strauss E (2012) The antibiotic CJ-15,801 is an antimetabolite that hijacks and then inhibits CoA biosynthesis, Chem. Biol. 19, 559–571. [PubMed: 22633408]

(25). Tonge PJ (2019) Quantifying the Interactions between Biomolecules: Guidelines for Assay Design and Data Analysis, ACS Infect. Dis. 5, 796–808. [PubMed: 30860805]

(26). Manoj N, Strauss E, Begley TP, and Ealick SE (2003) Structure of Human Phosphopantothenoylcysteine Synthetase at 2.3 Å Resolution, Structure 11, 927–936. [PubMed: 12906824]

(27). Zheng P, Zhang M, Khan MH, Liu H, Jin Y, Yue J, Gao Y, Teng M, Zhu Z, and Niu L (2019) Crystallographic Analysis of the Catalytic Mechanism of Phosphopantothenoylcysteine Synthetase from *Saccharomyces cerevisiae*, J. Mol. Biol. 431, 764–776. [PubMed: 30653991]

(28). Stanitzek S, Augustin MA, Huber R, Kupke T, and Steinbacher S (2004) Structural Basis of CTP-Dependent Peptide Bond Formation in Coenzyme A Biosynthesis Catalyzed by *Escherichia coli* PPC Synthetase, Structure 12, 1977–1988. [PubMed: 15530362]

(29). Mendes V, Green SR, Evans JC, Hess J, Blaszczyk M, Spry C, Bryant O, Cory-Wright J, Chan DSH, Torres PHM, Wang Z, Nahiyaan N, O'Neill S, Damerow S, Post J, Bayliss T, Lynch SL, Coyne AG, Ray PC, Abell C, Rhee KY, Boshoff HIM, Barry CE, Mizrahi V, Wyatt PG, and Blundell TL (2021) Inhibiting *Mycobacterium tuberculosis* CoaBC by targeting an allosteric site, Nat. Commun 12, 143. [PubMed: 33420031]

(30). Yaremchuk A, Kriklivyi I, Tukalo M, and Cusack S (2002) Class I tyrosyl-tRNA synthetase has a class II mode of cognate tRNA recognition, EMBO J. 21, 3829–3840. [PubMed: 12110594]

(31). Crooks GE, Hon G, Chandonia J-M, and Brenner SE (2004) WebLogo: A Sequence Logo Generator, Genome Res. 14, 1188–1190. [PubMed: 15173120]

(32). Iuso A, Wiersma M, Schüller H-J, Pode-Shakked B, Marek-Yagel D, Grigat M, Schwarzmayr T, Berutti R, Alhaddad B, Kanon B, Grzeschik NA, Okun JG, Perles Z, Salem Y, Barel O, Vardi A, Rubinshtein M, Tirosh T, Dubnov-Raz G, Messias AC, Terrile C, Barshack I, Volkov A, Avivi C, Eyal E, Mastantuono E, Kumbar M, Abudi S, Braunisch M, Strom TM, Meitinger T, Hoffmann GF, Prokisch H, Haack TB, Brundel BJJM, Haas D, Sibon OCM, and Anikster Y (2018) Mutations in PPCS, Encoding Phosphopantothenoylcysteine Synthetase, Cause Autosomal-Recessive Dilated Cardiomyopathy, Am. J. Hum. Genet. 102, 1018–1030. [PubMed: 29754768]

(33). Bosveld F, Rana A, van der Wouden PE, Lemstra W, Ritsema M, Kampinga HH, and Sibon OCM (2008) De novo CoA biosynthesis is required to maintain DNA integrity during development of the Drosophila nervous system, Hum. Mol. Genet. 17, 2058–2069. [PubMed: 18407920]

(34). Rana A, Seinen E, Siudeja K, Muntendam R, Srinivasan B, van der Want JJ, Hayflick S, Reijngoud D-J, Kayser O, and Sibon OCM (2010) Pantethine rescues a *Drosophila* model for pantothenate kinase–associated neurodegeneration, Proc. Natl. Acad. Sci. U.S.A. 107, 6988–6993. [PubMed: 20351285]

(35). Siudeja K, Grzeschik NA, Rana A, de Jong J, and Sibon OCM (2012) Cofilin/twinstar phosphorylation levels increase in response to impaired coenzyme A metabolism, PLoS One 7, e43145. [PubMed: 22912811]

(36). Noda S, Umezaki H, Yamamoto K, Araki T, Murakami T, and Ishii N (1988) Reye-like syndrome following treatment with the pantothenic acid antagonist, calcium hopantenate, J. Neurol. Neurosurg. Psychiatry 51, 582–585. [PubMed: 3379435]

(37). Noda S, Haratake J, Sasaki A, Ishii N, Umezaki H, and Horie A (1991) Acute encephalopathy with hepatic steatosis induced by pantothenic acid antagonist, calcium hopantenate, in dogs, Liver 11, 134–142. [PubMed: 1886458]

(38). Smashevskii ND, Kopelevich VM, and Gunar VI (1986) Antivitamin effect of D-homopantothenic acid on higher plants, Fiziol. Rast. Genet. 33, 1138–1143.

(39). Robishaw JD, and Neely JR (1984) Pantothenate kinase and control of CoA synthesis in heart, Am. J. Physiol. Heart Circ. Physiol. 246, H532–H541.

(40). Strauss E, Kinsland C, Ge Y, McLafferty FW, and Begley TP (2001) Phosphopantothenoylcysteine Synthetase from Escherichia coli : IDENTIFICATION AND CHARACTERIZATION OF THE LAST UNIDENTIFIED COENZYME A BIOSYNTHETIC ENZYME IN BACTERIA, J. Biol. Chem. 276, 13513–13516. [PubMed: 11278255]

(41). Daugherty M, Polanuyer B, Farrell M, Scholle M, Lykidis A, de Crécy-Lagard V, and Osterman A (2002) Complete Reconstitution of the Human Coenzyme A Biosynthetic Pathway via Comparative Genomics, J. Biol. Chem. 277, 21431–21439. [PubMed: 11923312]

(42). Kabsch W (2010) Xds, Acta Crystallogr. D. 66, 125–132. [PubMed: 20124692]

(43). McCoy AJ, Grosse-Kunstleve RW, Adams PD, Winn MD, Storoni LC, and Read RJ (2007) Phaser crystallographic software, J. Appl. Crystallogr. 40, 658–674. [PubMed: 19461840]

(44). Winn MD, Ballard CC, Cowtan KD, Dodson EJ, Emsley P, Evans PR, Keegan RM, Krissinel EB, Leslie AG, McCoy A, McNicholas SJ, Murshudov GN, Pannu NS, Potterton EA, Powell HR, Read RJ, Vagin A, and Wilson KS (2011) Overview of the CCP4 suite and current developments, Acta Crystallogr. D. 67, 235–242. [PubMed: 21460441]

(45). Vagin AA, Steiner RA, Lebedev AA, Potterton L, McNicholas S, Long F, and Murshudov GN (2004) REFMAC5 dictionary: organization of prior chemical knowledge and guidelines for its use, Acta Crystallogr. D. 60, 2184–2195. [PubMed: 15572771]

(46). Emsley P, and Cowtan K (2004) Coot: model-building tools for molecular graphics, Acta Crystallogr. D. 60, 2126–2132. [PubMed: 15572765]

(47). Emsley P, Lohkamp B, Scott WG, and Cowtan K (2010) Features and development of Coot, Acta Crystallogr. D. 66, 486–501. [PubMed: 20383002]

(48). Morris GM, Huey R, Lindstrom W, Sanner MF, Belew RK, Goodsell DS, and Olson AJ (2009) AutoDock4 and AutoDockTools4: Automated docking with selective receptor flexibility, J. Comput. Chem. 30, 2785–2791. [PubMed: 19399780]

(49). Shi L, and Tu BP (2013) Acetyl-CoA induces transcription of the key G1 cyclin *CLN3* to promote entry into the cell division cycle in *Saccharomyces cerevisiae*, Proc. Natl. Acad. Sci. U.S.A. 110, 7318–7323. [PubMed: 23589851]

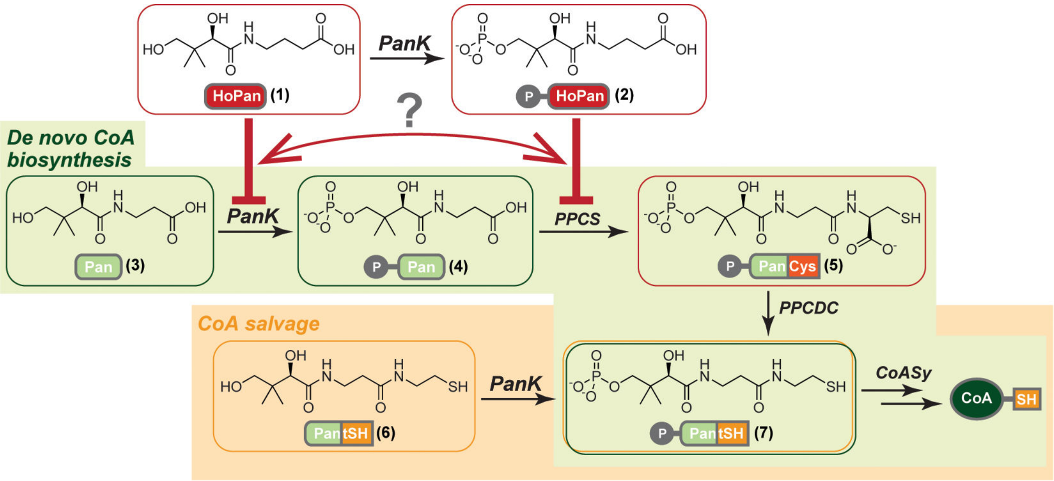

Figure 1. Coenzyme A (CoA) biosynthesis and the proposed molecular targets of HoPan.

In humans and *D. melanogaster* CoA is biosynthesized *de novo* from Pan in a five-step pathway (boxed in green) catalyzed by pantothenate kinase (PanK), phosphopantothenoylcysteine synthetase (PPCS), phosphopantothenoylcysteine decarboxylase (PPCDC) and the bifunctional CoA synthase (CoASy) that has both phosphopantetheine adenylyltransferase (PPAT) and dephospho-CoA kinase (DPCK) activity. It can also be salvaged from pantetheine (PantSH), a CoA degradation product (pathway boxed in orange), through dual action of many PanKs. The possible targets for HoPan's inhibition of CoA biosynthesis are indicated; this study aims to distinguish between these possibilities.

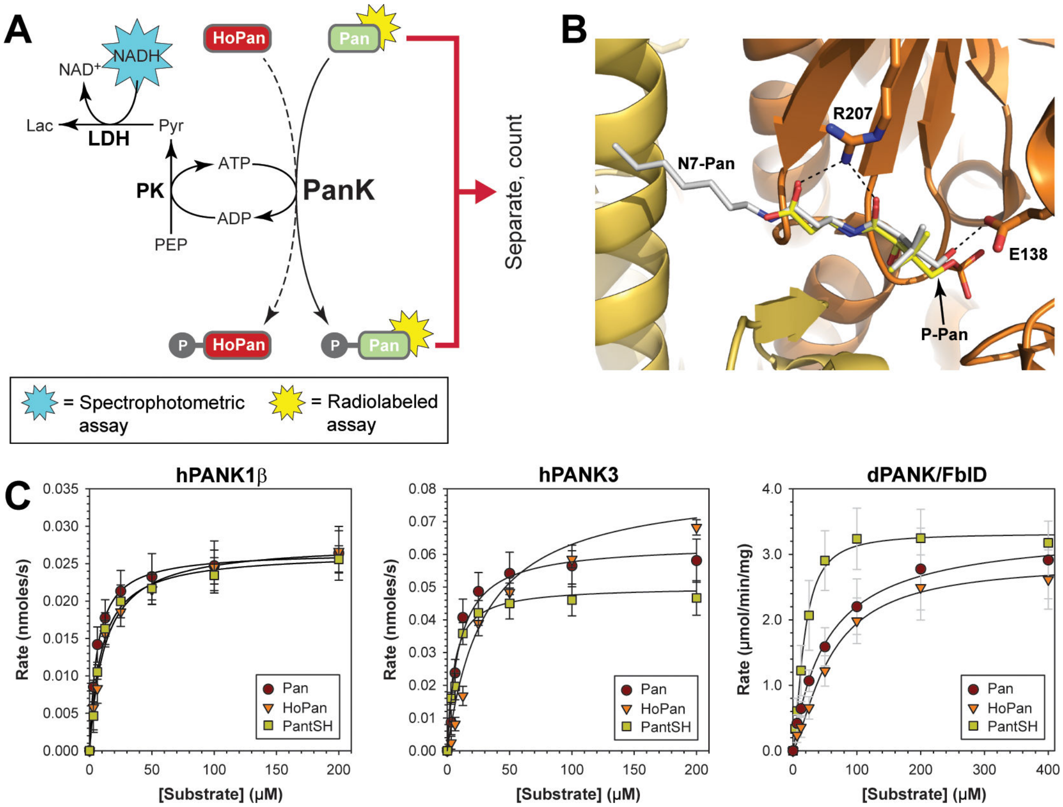

Figure 2. Activity characterization of human and fruit fly PanK isoforms.

(**A**) Schematic representation of the two PanK activity assays that are usually used: a discontinuous *radiolabeled* assay that determines the amount of radiolabeled P-Pan formed from radiolabeled ([^{13}C]) Pan following separation of the product and unreacted substrate, which is blind to the enzyme acting on other substrates, and a *spectrophotometric* assay that couples the conversion of ATP to ADP to the oxidation of NADH using the pyruvate kinase (PK) and lactate dehydrogenase (LDH) reactions, which measures kinase activity towards all substrates without distinction. (**B**) Active site of hPANK3 with the PantSH analogue N7-Pan (stick structure with carbon atoms in white) bound (PDB: 3SMS). The two subunits of the dimeric enzyme are shown in different shades of orange; the loop covering the active site is not shown for the sake of clarity. Residue E138 involved in catalysis and R207 involved in positioning the substrate are indicated. Also shown is the PanK reaction product P-Pan (stick structure with carbon atoms in yellow) obtained by overlaying the structure of hPANK3 bound to P-Pan and ADP (PDB: 5KPZ[23]). (**C**) Activity profiles obtained for (from left to right) hPANK1β, hPANK3 and dPANK/FblD with Pan, HoPan and PantSH as substrates. The symbols in the activity profiles are the average values obtained at the indicated concentration in at least three independent experiments. The error bars indicate the SEM of the averaged data. The solid line represents the fit to the Michaelis-Menten or Hill equations (see Table 1). For dPANK/FblD, different batches of enzyme gave different levels of specific activity (suggesting poor stability); in its case the rates are therefore reported relative to the amount of protein used to highlight this variability.

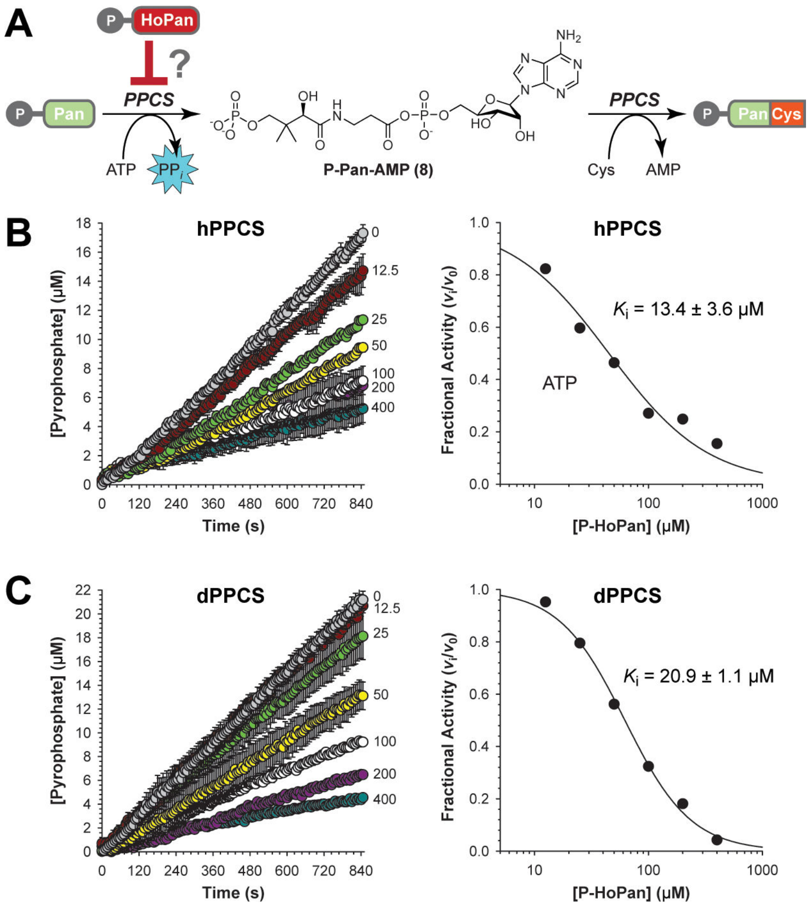

Figure 3. P-HoPan inhibits human and fruit fly PPCS enzymes.

(**A**) Mechanism of eukaryotic PPCS enzymes, showing formation of the 4′-phosphopantothenoyl adenylate (P-Pan-AMP) intermediate from P-Pan in the first step with concomitant release of pyrophosphate (PP$_i$), and the reaction of the intermediate with L-cysteine and release of AMP in the second step to from the product P-PanCys. The possible inhibition of PPCS by P-HoPan was studied by tracking the rate of PP$_i$ release using an assay that couples its formation to the oxidation of NADH. (**B**) On the left, progress curves for hPPCS with 150 μM P-Pan, 1 mM L-cysteine and 1 mM ATP and increasing concentrations of P-HoPan (concentrations in μM indicated on the right of each curve). Symbols indicate the average of duplicate readings, and the error bars show range/2. On the right, fractional activity (v_i/v_0) of hPPCS at each P-HoPan concentration as calculated from the progress curves, allowing for an IC$_{50}$ value to be determined. The IC$_{50}$ value was converted to the indicated K_i value using the Cheng-Prusoff equation for competitive inhibitors (Eqn. 4). The K_i value is the average from two independent experiments, the error is the range/2. (**C**) As for **B**, but with dPPCS.

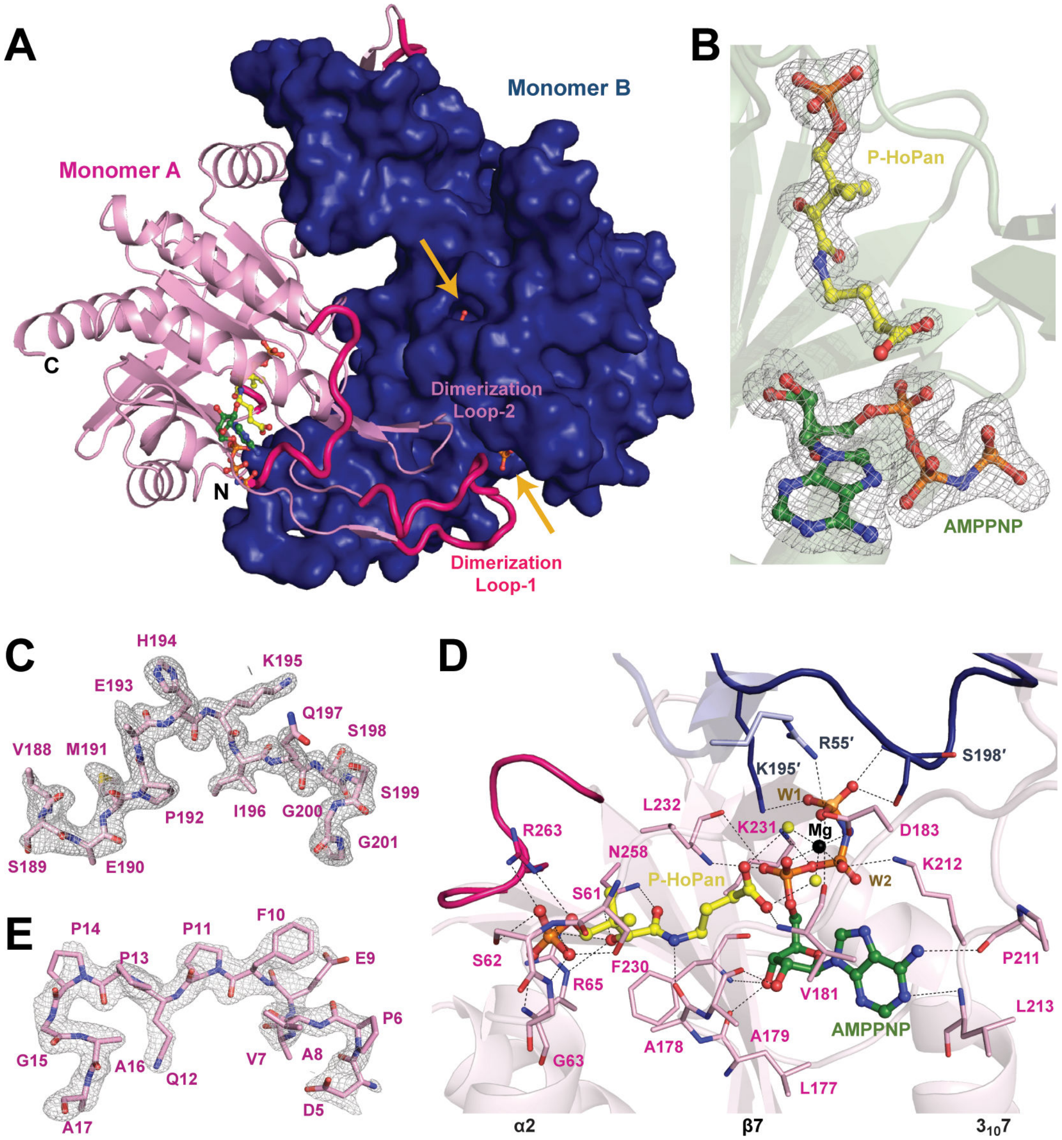

Figure 4. The crystal structure of hPPCS with P-HoPan and AMPPNP bound is highly ordered, revealing previously unseen active site interactions.

(**A**) Overview of the overall dimeric crystal structure of hPPCS. One monomer is depicted as a dark blue surface, the other as a pink cartoon. The ligands AMPPNP (dark green) and P-HoPan (yellow) are represented in ball and stick view. The solvent accessible phosphate groups of P-HoPan and AMPPNP are highlighted by orange arrows. Thick loops (magenta) represent the regions that were disordered in all previous PPCS structures, and are observed here for the first time. (**B**) Electron densities of AMPPNP and P-HoPan generated from mF_o-DF_c map contoured at 2.5 σ. (**C**) Electron density of the ordered dimerization loop-1 (residues 188–201) involved in capping the ligand generated from the mF_o-DF_c map contoured at 2.5 σ. (**D**) Global view of the hPPCS active site pocket with all residues present at hydrogen-bonding distance from AMPPNP and P-HoPan. The newly ordered loops are highlighted in hot pink (from one monomer) and blue (from neighbouring monomer). Residues from different monomers are shown by pink and blue sticks respectively. A magnesium ion (Mg) is represented by a black sphere and water molecules W1 and W2 by yellow spheres. (**E**) Electron density of the ordered flexible flap (residues 259−265) involved in capping the ligand generated from the mF_o-DF_c map contoured at 2.5 σ.

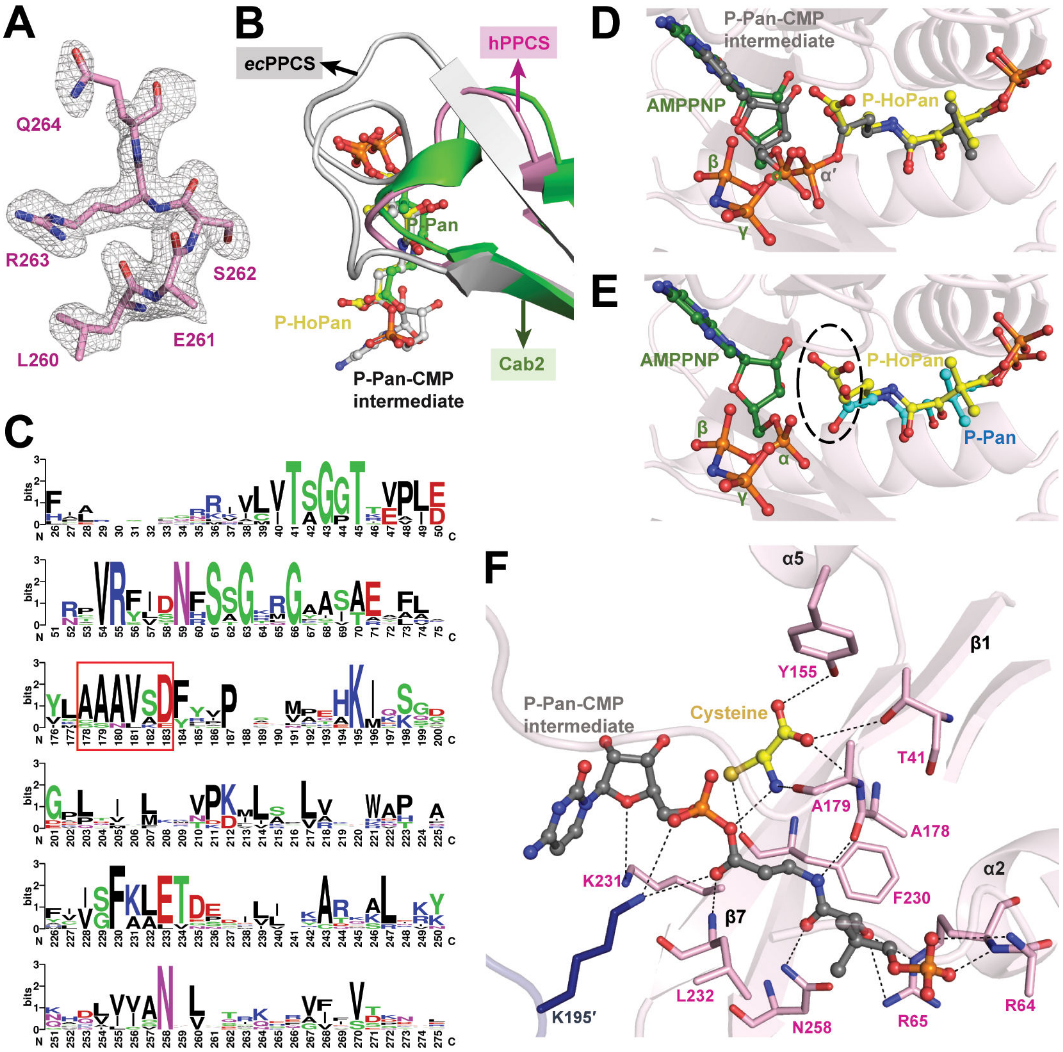

Figure 5. Comparison of the hPPCS ternary complex with *E. coli* PPCS and Cab2 structures reveals the inhibition mechanism of P-HoPan.

(**A**) Electron density of the ordered N-terminal loop (residues 5–17) generated from the mF_o-DF_c map contoured at 2.5 σ. (**B**) Comparison of the substrate-binding site in hPPCS (pink), *E. coli* PPCS (*ec*PPCS; grey) and Cab2 (green). In the case of *ec*PPCS, the loop is longer (from residue D354 to N367) than in hPPCS and Cab2. P-HoPan, the P-Pan-CMP intermediate and P-Pan are shown in yellow, grey and green ball and stick view. (**C**) Sequence logo representation of an alignment of selected PPCS sequences (human, mouse, *Arabidopsis thaliana*, *D. melanogaster*, *Oryza sativa*, *S. cerevisiae* (i.e Cab2), *Mycobacterium tuberculosis*, *Streptococcus pneumoniae*, *S. aureus* and *E. coli*); only a portion of the sequence is shown to highlight the consensus motifs and conserved residues—including the 'AAV(A/S)D' motif associated with nucleotide binding and proposed to be involved in binding of cysteine (red box). The overall height of the letter stack indicates the sequence conservation at that position, while the height of each letter within the stack indicates the relative frequency of each amino acid at that position. Numbering according to hPPCS. Gaps in the alignment, where present, were omitted for clarity. Figure prepared using Weblogo.[31] (**D**) Overlay of AMPPNP in the hPPCS structure with P-Pan (cyan ball and stick structure) from the Cab2 structure (PDB: 6AI9[27]) and P-Pan-CMP intermediate (dark grey ball and stick structure) from *ec*PPCS (PDB: 1U7Z[28]). (**E**) Overlay of AMPPNP and P-HoPan in the hPPCS structure with P-Pan from the Cab2 structure (PDB: 6AI9). The different conformations of the P-Pan and P-HoPan carboxylate groups is highlighted by the dashed line ellipse. (**F**) The cysteine binding site was modelled in the ternary hPPCS complex using AutoDock 4.2. The P-Pan-CMP intermediate was probed into the active site using the co-ordinates of the structure of Cab2 with the intermediate bound (PDB: 6AIK[27]). The intermediate and cysteine are shown in gray and yellow ball and stick view, respectively. The residues shown in pink sticks are from one monomer, while those shown in blue is from the neighbouring monomer's dimerization loop.

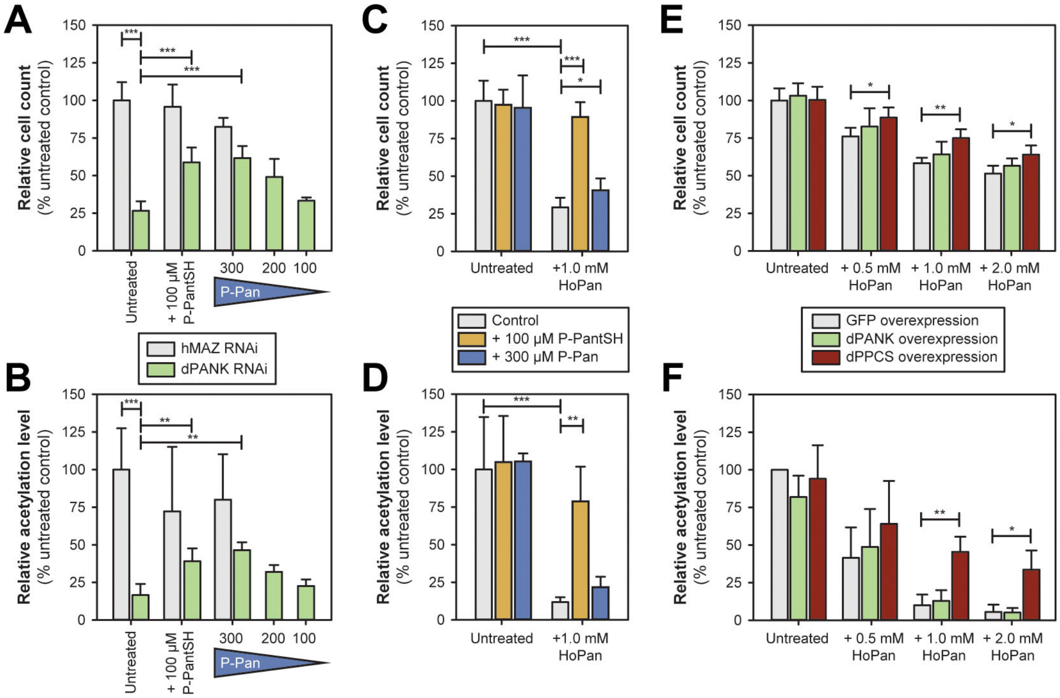

Figure 6. HoPan targets PPCS in *D. melanogaster* Schneider's S2 cells.

(**A**) Relative cell counts in cultured *Drosophila* S2 cells treated with control dsRNA (directed against hMAZ, a non-relevant human gene) or with dsRNA against dPANK/Fbl, and subsequent rescue through the addition of 100 µM P-PantSH or P-Pan (300 µM, 200 µM or 100 µM). (**B**) Effect on histone acetylation (relative to tubulin) in the samples shown in **A**. (**C**) Relative cell counts in untreated control cells or cells treated with 1 mM HoPan, and the subsequent rescue of the effects of HoPan treatment by addition of either 100 µM P-PantSH or 300 µM P-Pan. (**D**) Effect on histone acetylation (relative to tubulin) in the samples shown in **C**. (**E**) Relative cell counts of S2 cells overexpressing a control construct (GFP), or overexpressing either dPANK/Fbl or dPPCS, and the effects of increasing amounts of HoPan under these conditions. (**F**) Effect on histone acetylation (relative to tubulin) in the cells under the indicated conditions as shown in **E**. Data represent mean ± s.d. (n ≥ 3). *P ≤ 0.05, **P ≤ 0.01, ***P ≤ 0.001, two-tailed unpaired Student's t-test.

Table 1.

Kinetic parameters for PanKs with its natural substrate Pan, the salvage pathway precursor PantSH and the putative CoA biosynthesis inhibitor HoPan.[a]

PanK	Substrate	K_M or $K_{0.5}$ (μM)	k_{cat} (s^{-1})	k_{cat}/K_M or $k_{cat}/K_{0.5}$ ($mM^{-1}.s^{-1}$)	N [b]	Equation fitted[c]	R^2 value[d]
hPANK1β	Pan	6.20 ± 0.88	0.23 ± 0.03	38.1 ± 7.1	3	MM	0.9975
	HoPan	12.1 ± 1.9	0.24 ± 0.02	21.1 ± 4.6	3	MM	0.9927
	PantSH	9.85 ± 1.17	0.23 ± 0.02	24.1 ± 4.3	3	MM	0.9888
hPANK3	Pan	10.9 ± 1.4	0.53 ± 0.14	52.9 ± 10.6	5	MM	0.9753
	HoPan	36.2 ± 2.1 28.6 ± 3.2	0.67 ± 0.02 0.63 ± 0.10	19.5 ± 1.6 22.7 ± 1.9	5	MM Hill (n = 1.32 ± 0.18)	0.9868 0.9922
	PantSH	8.05 ± 1.87 7.12 ± 1.33	0.41 ± 0.13 0.47 ± 0.03	57.6 ± 24.6 72.0 ± 14.0	4	MM Hill (n = 1.81 ± 0.24)	0.9875 0.9968
dPANK/FblD	Pan	52.2 ± 4.0	2.79 ± 0.62	52.5 ± 8.7	4	MM	0.9987
	HoPan	82.2 ± 12.4 60.3 ± 3.9	2.72 ± 0.50 2.38 ± 0.43	35.6 ± 8.4 40.6 ± 8.3	4	MM Hill (n = 1.47 ± 0.32)	0.9887 0.9961
	PantSH	28.9 ± 13.0 19.3 ± 6.6	3.24 ± 0.45 2.46 ± 0.66	169 ± 84 145 ± 43	4	MM Hill (n = 2.01 ± 0.57)	0.9760 0.9939

[a] Reported parameters are the average values of the parameters obtained from the indicated number of experiments. For each experiment, the parameters were obtained by fitting the indicated equation to the data obtained in triplicate. The indicated error is the standard error of the mean.

[b] Number of individual experiments, each performed in triplicate.

[c] MM refers to the Michaelis-Menten equation given in Eqn. 1. In cases where cooperativity was observed (evidence of sigmoidal activity profiles), the Hill equation (Eqn. 2) was also fit to the data. In these cases, the K_M value is $K_{0.5}$, and the obtained Hill coefficient (n) is given.

[d] R^2 value for the indicated equation fitted to the data averaged from all the experiments; fitting the data to the Hill equation invariably indicates a better fit due to the introduction of the third parameter (the Hill coefficient).